Research Article

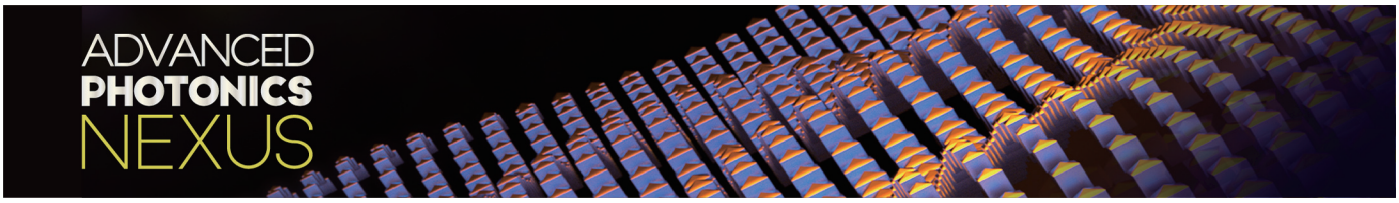

Anomalous broadband Floquet topological metasurface with pure site rings

Zhiwei Guo,[a,*] Xian Wu,[a] Yong Sun,[a,*] Haitao Jiang,[a] Ya-Qiong Ding,[b] Yunhui Li,[a] Yewen Zhang,[a] and Hong Chen[a,*]

[a]Tongji University, Key Laboratory of Advanced Microstructure Materials, School of Physics Science and Engineering, Shanghai, China
[b]University of Shanghai for Science and Technology, Science College, Shanghai, China

Abstract. Photonic and acoustic topological insulators exhibiting one-way transportation that is robust against defects and impurities are typically realized in coupled arrays of two-dimensional ring resonators. These systems have produced a series of applications, including optical isolators, delay lines, and lasers. However, the structures are complicated because an additional coupler ring between neighboring rings is needed to construct photonic pseudospin. A photonic anomalous Floquet topological insulator is proposed and experimentally demonstrated in the microwave regime. This improved design takes advantage of the efficient and backward coupling of negative-index media. The results contribute to the understanding of topological structures in metamaterials and point toward a unique direction for constructing useful topological photonic devices.

Keywords: topological edge states; circuit-based metamaterials; backward coupling; topological photonics.

Received Oct. 11, 2022; revised manuscript received Nov. 20, 2022; accepted for publication Dec. 6, 2022; published online Jan. 2, 2023.

[DOI: 10.1117/1.APN.2.1.016006]

1 Introduction

Edge modes of photonic topological insulators, which travel along the boundary of the structure and are robust against perturbations, have recently become a subject of much interest.[1–3] Although early designs for photonic topological one-way edge modes involved breaking the time-reversal (T-reversal) symmetry in gyromagnetic materials using an external magnetic field,[4–7] it was soon discovered that a synthetic magnetic field could exhibit the same effect as a real magnetic field in producing one-way edge modes.[8–10] Much like the topological insulators in electric systems,[11,12] T-reversal symmetry preserved photonic systems with nontrivial topological phases have attracted considerable interest from researchers. Such systems have been realized in a variety of structures, including bi-anisotropic metamaterials,[13–17] photonic crystals,[18–23] and arrays of coupled ring resonators (CRRs).[24–36] Great progress in topological photonics has extended its scope from microwave to X-ray frequencies,[37] passive to active structures,[38,39] near-field to far-field measurement,[40,41] short-range to long-range coupling,[42–44] one to higher dimensions,[45–47] and classical to quantum optics.[48–50]

Diversified CRR arrays, which provide a suitable platform for the study of topological photonics, have received substantial attention. The roles of pseudospins in opposite directions are played by the clockwise and anticlockwise propagation directions of light.[24–32] High-performance topological optical devices based on CRR arrays, such as delay lines,[24] optical isolators,[28] and lasers,[31,32] have been proposed as key components for optical communication systems. Liang and Chong[26] demonstrated theoretically that a lattice of optical ring resonators can exhibit a topological insulator phase even if all bands have a zero Chern number. Unlike earlier designs that required delicately tuning the aperiodic couplings of the interresonators,[24,25] this simplified structure is periodic and contains identical CRRs.[26,27] Inspired by this anomalous Floquet topological insulator, topological edge states with T-symmetry have been experimentally measured using a surface plasmon structure.[30] This novel topological edge mode has also been demonstrated in acoustic systems.[51,52]

*Address all correspondence to Zhiwei Guo, 2014guozhiwei@tongji.edu.cn; Yong Sun, yongsun@tongji.edu.cn; Hong Chen hongchen@tongji.edu.cn

However, the coupling between the site rings in CRR arrays needs to be very strong for the realization of an anomalous Floquet topological insulator.[26] At present, the typical solution is to insert a coupler ring between two site rings. Achieving strong coupling relies on the resonance of the coupler ring, which severely limits the bandwidth of the strong coupling regime.[29] In addition, the CRR array design is complicated by the requirement of an additional coupler ring between the nearest neighboring rings to construct the photonic pseudospin.[24–36] Thus, a question naturally arises: can an anomalous Floquet topological insulator be constructed without additional coupler rings and with a broad bandwidth? In particular, Afzal et al.[53,54] theoretically proposed and experimentally demonstrated that the anomalous Floquet insulators, in which the unit cell was composed of four CRRs, can occur using a square lattice of direct-coupled octagonal resonators, owing to the unequal synchronous coupling and asynchronous coupling. Their remarkable findings discovered that the natural spin flipping can be used to realize the anomalous Floquet topological insulators.

Metamaterials/metasurfaces, artificial materials composed of subwavelength unit cells, provide a powerful platform for manipulating the propagation of light. The backward and efficient coupling mechanism of left-handed media (LHM) can also be used to solve the above problems.[55–58] Recently, high-performance metasurfaces have been constructed to achieve the required optical response in transmission line (TL) platforms and have enabled extensive applications, such as cloaking,[59] hyperbolic dispersion,[60,61] quantum-optics-like phenomena,[62,63] and topological photonics.[21] Utilizing a TL system, in this work we design circuit-based negative-index media in the microwave regime. An improved anomalous Floquet topological insulator is constructed from a square array of CRRs composed of composite right/left-handed (CRLH) TLs. In each individual ring resonator, the roles of opposite pseudospins are played by the clockwise and anticlockwise propagation of electromagnetic waves. A directional coupler inserted into the site rings supports backward wave coupling without requiring additional coupler rings. A photonic anomalous Floquet topological metasurface with pure site rings is observed in both numerical simulations and experiments. We also investigate the robustness of edge states against perturbations in the structure. For the anomalous Floquet topological insulator, CRR array design is usually complicated because it needs to add a coupler ring between the nearest adjacent rings to construct photon pseudo-spin. Therefore, the anomalous Floquet topological metasurface with pure site rings shown in this work looks simpler because there are fewer rings. Our findings not only provide a useful understanding for studying topological structures using metamaterials, but also may offer a new means of realizing topological photonic devices.

2 Design and Method

The near-field directional coupling between resonance rings plays an important role in the realization of Floquet topological structures.[24–28] The novel negative refractive property of LHM can serve in the abnormal backward coupling. For the rings with normal right-handed material (RHM), the conservation condition of the tangential wave vector imposes forward coupling for the RHM rings, as shown schematically in Fig. 1(a). It can be clearly seen that the pseudo-spin will flip in a forward coupling; thus, a coupled ring needs to be inserted between the site rings to ensure that the pseudospin in the site rings is maintained. However, the coupling direction is reversed when one of the rings is composed of LHM, as schematically shown in Fig. 1(b). As opposed to the forward coupling shown in Fig. 1(a), the backward-coupling-enabled consistent pseudospin in site rings paves a new way to design topological structures.

In the circuit-based system, the relationship between the electric and magnetic fields can be easily mapped using the relationship between voltage and current. As a result, the electromagnetic response is equivalent to the circuit parameters. The structure factor of the TL is defined as $g = Z_0/\eta_{\text{eff}}$, where Z_0 and η_{eff} denote the characteristic impedance and effective wave impedance, respectively. For the TL model of the LHM in Fig. 2(a), the structure factor is $g = [1.393 + w/h + 0.667\ \ln(w/h) + 1.444]^{-1}$. The impedance and admittance of the circuit are represented by Z and Y, respectively. The direction of the magnetic field produced by the current can be determined from Ampere's law, as shown in Fig. 2(b). By mapping the circuit equation (telegraph equation) to Maxwell's equations, the relationship between circuit and electromagnetic parameters can be described by $\mu_{\text{eff}}\mu_0 g = Z/i\omega$ and $\varepsilon_{\text{eff}}\varepsilon_0/g = Y/i\omega$, respectively. ε_0 and μ_0 are the vacuum permittivity

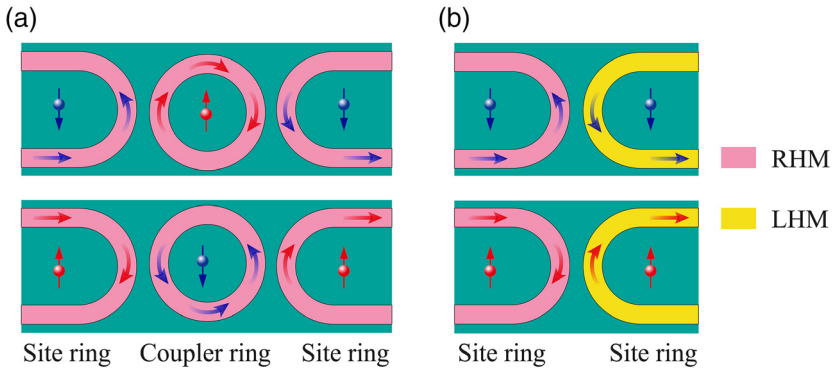

Fig. 1 Schematics of the photonic pseudospin in the coupled ring system. (a) Reversal of pseudo-spin in forward coupling. (b) Consistency of pseudo-spins in the process of backward coupling. The upper (lower) row denotes pseudo-spin-down (up) mode. RHM and LHM are marked by pink and yellow, respectively.

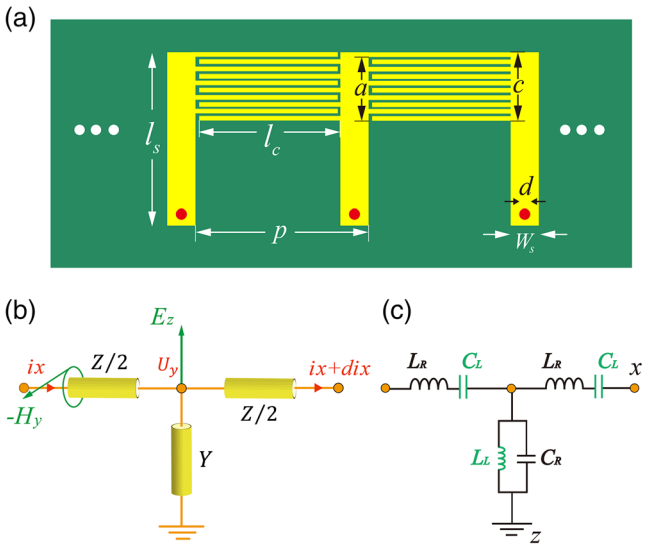

Fig. 2 Realization of circuit-based LHM. (a) Schematic of circuit-based LHM realized in the TL platform; the structural parameters are given in Supplementary Material. (b) TL model of the circuit-based LHM. (c) Corresponding circuit model of the effective LHM.

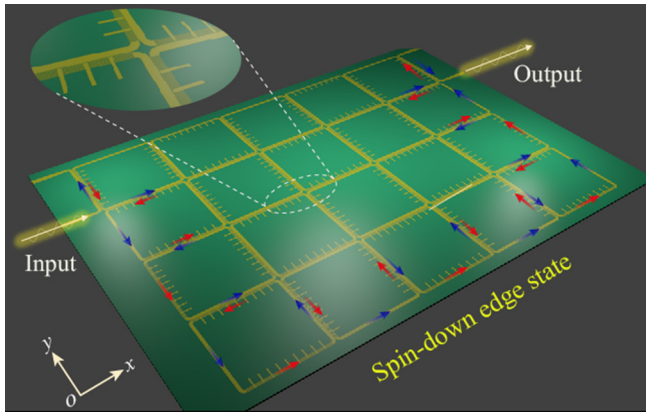

Fig. 3 Schematic of anomalous Floquet topological insulator based on CRLH ring resonators. The size of our fabricated sample is 4 × 5 unit cells. The RHM (simple line strips) and left-handed material (complex branched strips) connect successively in a ring structure. The zoom-in picture of different ring resonators is presented on the top. The arrows represent the coupling direction of the energy flow in two materials with different handedness. The upper metallic microstrip and the lower dielectric substrate are marked by yellow and green, respectively.

and permeability, respectively. ω is the angular frequency. The effective permittivity and permeability of the circuit system can be tuned using the lumped elements in the circuit. Figure 2(c) shows a simple effective circuit model for a circuit-based hyperbolic metamaterial. In this circuit model, the admittance and impedance are $Y = i\omega C_R + 1/i\omega L_L$ and $Z = i\omega L_R + 1/i\omega C_L$, respectively. C_R and L_R denote the capacitance and inductance per unit length, respectively. Therefore, the effective electromagnetic parameters of the circuit-based LHM are $\varepsilon_{\text{eff}} = (C_R - 1/\omega^2 \cdot L_L)g/\varepsilon_0$ and $\mu_{\text{eff}} = (L_R - 1/\omega^2 \cdot C_L)/g\mu_0$, respectively. Especially, the LHM can be realized when $\varepsilon_{\text{eff}} < 0$ and $\mu_{\text{eff}} < 0$.

A schematic of an array of CRLH ring resonators forming an anomalous Floquet topological insulator is shown in Fig. 3. Distributed CRLH TLs[54,55] are used to design a LHM with a negative refraction index. The ring resonator can then be constructed by connecting left- and right-handed TLs in sequence. A square array of coupled CRLH ring resonators can be produced by arranging the resonators in close proximity. The size of the fabricated sample is 340.4 mm × 272.3 mm. Unlike previous anomalous Floquet topological insulators, in which additional resonators were adopted as coupler rings,[24–36] every ring resonator in the improved platform belongs to a site ring, as shown in Fig. 3. Two U-shaped waveguides serve as input and output ports. In the improved platform, the site rings are backward-coupled with their neighbors through the vortex-like interface mode existing in the CRLH coupler, as shown in Fig. 1(b). This provides considerable advantages, such as high coupling strength and broad bandwidth.[55–58] It is the mechanism of backward coupling that prevents the electromagnetic waves from being coupled back to the input ring after one coupling process, which greatly increases the coupling efficiency.[55–58] Additional coupler rings are not required in anomalous Floquet topological insulators based on left-handed metamaterials. Details of the structural parameters, effective circuit models, and the design scheme of the negative-index media are given in the Supplementary Material. When circular ring is considered instead of square ring in Fig. 3, the coupling of adjacent rings will change from line coupling to point coupling, which leads to the characteristics of narrowband coupling. As a result, the number of bandgaps will also change. Especially, it should be emphasized that when considering other shapes with effective line coupling, such as octagonal ring resonators,[53,54] the related results are maintained.

The band structure of the proposed array of CRLH ring resonators can be calculated as follows. A schematic of the coupling network constructed by resonance rings is shown in Fig. 4(a). The position of the resonance rings and the relationship between the wave amplitudes are indicated by square green boxes and red arrows, respectively. To determine the backward coupling between RHM and LHM waveguides, we first study the simple configuration of thre $U-U$ waveguide structure, as shown in Fig. 4(b). Using the computer simulation technology Microwave Studio software, the backward coupling is simulated; the corresponding electric field distribution is shown in Fig. 4(c). The amplitudes of the waves in the ring resonators are expressed in the form of a scattering matrix[26],

$$S(\theta,\chi) = e^{i\chi}\begin{bmatrix} \sin\theta & i\cos\theta \\ i\cos\theta & \sin\theta \end{bmatrix}, \tag{1}$$

where θ denotes the coupling strength between adjacent lattice rings and χ is the overall phase factor. The highly dispersive behavior of θ, plotted in Fig. 4(d), is written as

$$\theta = \sin^{-1}[(I_{\text{out}}/I_{\text{in}})^{1/2}], \tag{2}$$

which is derived from the $U-U$ shape structure in Fig. 4(c). I_{in} and I_{out} denote the power through the incident and transmitted waveguides, respectively. The green region marked in Fig. 4(d) covers the frequency range for strong coupling, where $\theta > \pi/4$; the nontrivial topological phase exists in this range.[26–30] Edge states can be observed in a semi-infinite strip-coupled rings lattice, whose width is finite in the y direction and periodic

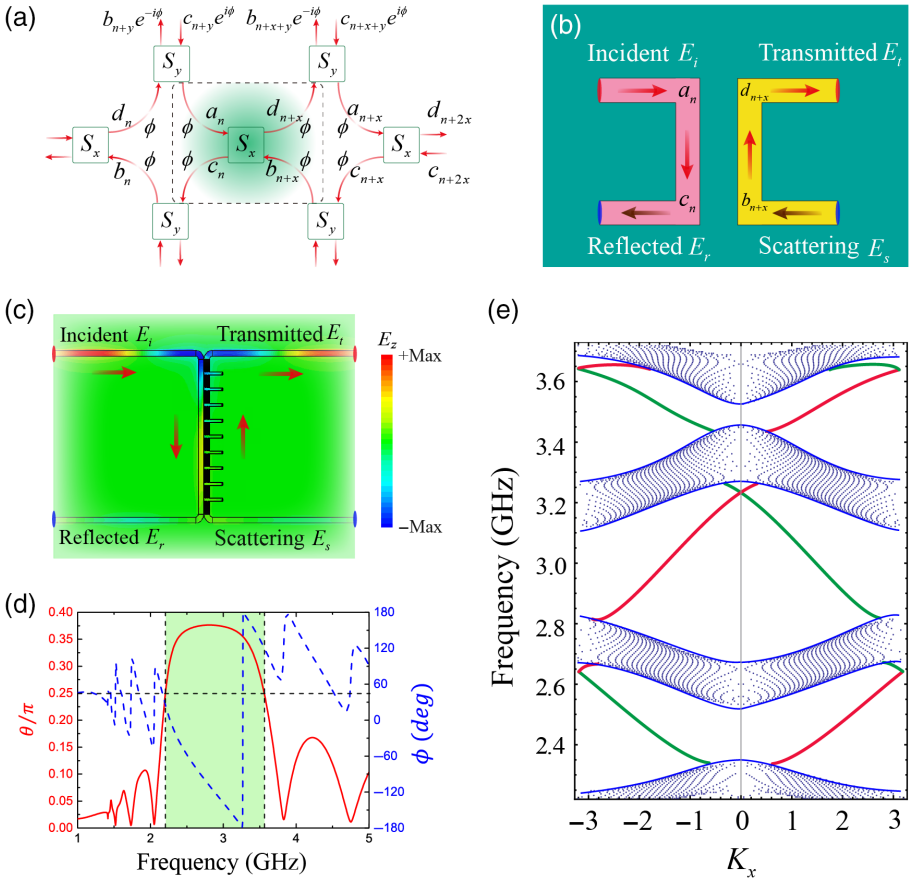

Fig. 4 Band structure and the edge states of the anomalous Floquet topological insulator. (a) Schematic of couplings between neighboring resonance rings, where the wave amplitude relations are marked by red arrows. (b) Configuration of $U-U$ waveguide structure. The incident wave with high performance is coupled to the transmitted port based on the wave vector conservation condition for back direction. (c) Simulated backward coupling between RHM and LHM waveguides. (d) The value of coupling strength θ (red line) and the corresponding coupling phase (blue dashed line) can be derived from the $U-U$ shape structure. (e) The projected band diagram of a semi-infinite strip-coupled ring lattice, whose width is finite in the y direction ($N=30$) and periodic in the x direction. Gapless edge modes periodically appear in the bandgap range of the infinite periodic structure. Red and green lines denote edge states corresponding to the upper and lower edges of the sample, respectively.

in the x direction. The positions of lattice rings are indicated by $n=(x_n,y_n)$, where x_n and y_n are the column and row indices, respectively. The coupling between the lattice rings at sites n and $n+x$ ($n+y$) in the x (y) direction is expressed by the scattering matrices S_x (S_y),

$$S_x\begin{bmatrix}a_n\\ b_{n+x}\end{bmatrix}=\begin{bmatrix}d_{n+x}\\ c_n\end{bmatrix}, S_y\begin{bmatrix}d_n\\ c_{n+y}\end{bmatrix}=\begin{bmatrix}b_{n+y}\\ a_n\end{bmatrix}e^{-2i\phi}, \tag{3}$$

where ϕ denotes the phase delay accumulated in the propagation through a quarter-lattice ring. The Bloch condition can be applied in the x direction for the periodic condition $|\varphi_{n+x}\rangle=e^{iK_x}|\varphi_n\rangle$. Combining this with the boundary conditions in the y direction, $c_1=e^{-2i\phi}b_1$ and $a_N=e^{2i\phi}d_N$, the equation for the eigenvalues is obtained[26],

$$\begin{bmatrix}M_1^x & & & \\ & M_2^x & & \\ & & \cdots & \\ & & & M_N^x\end{bmatrix}\cdot\begin{bmatrix}e^{-2i\phi} & & & \\ & M_1^y & & \\ & & \cdots & \\ & & & M_{N-1}^y & \\ & & & & e^{2i\phi}\end{bmatrix}\cdot\psi = e^{iK_x}|\Psi\rangle, \tag{4}$$

where $|\psi\rangle=[b_1d_1\cdots b_Nd_N]^{\mathrm{T}}$ and the submatrices are

$$M_i^x=\begin{bmatrix}\csc\theta & -i\cot\theta\\ i\cot\theta & \csc\theta\end{bmatrix}\quad(i=1,2,\ldots,N),$$
$$M_j^y=\begin{bmatrix}ie^{2i\phi}\sec\theta & -i\tan\theta\\ i\tan\theta & -ie^{-2i\phi}\sec\theta\end{bmatrix}\quad(j=1,2,\ldots,N-1). \tag{5}$$

According to Eqs. (4) and (5), gapless edge modes appear in the bandgap range, as shown in Fig. 4(e). The red and green lines denote edge states corresponding to the upper and lower edges. The emergence of a topological edge state is one of the most striking properties of topological insulators. Anomalous Floquet topological metasurfaces in all three different frequency bandgap ranges belong to a topological nontrivial phases. Due to the topological protection, edge states in three different frequency bandgap ranges have robust transmission characteristics that the electromagnetic waves can still propagate along the rugged boundary with little reflection.

We next demonstrate the improved photonic anomalous Floquet topological insulator. Each individual ring resonator possesses twofold degenerate modes, corresponding to a twofold pseudo-spin degree of freedom in which the clockwise and anticlockwise propagation directions of light play the role of the opposite pseudo-spins. By choosing the appropriate input port, clockwise and anticlockwise circulating photonic modes (e.g., two types of pseudospin) can be selected. As a result, two one-way edge modes can be excited along opposite directions. Figure 5 shows the results of full wave simulations of the electric field (E_z) distributions of the edge states. When the upper arm of the incident U-shaped waveguide [marked by the red arrow in Fig. 5(a)] is selected as the input port, the spin-up edge mode is excited with a working frequency of 2.5 GHz. Owing to the spin–orbit coupling, the wave is transmitted to the output port only along the upper portion of the array structure. The electric field distribution of the E_z component is shown in Fig. 5(a). Similarly, when the lower arm of the incident U-shaped waveguide [marked by the blue arrow in Fig. 5(b)] is chosen as the input port, the spin-down edge mode is selectively excited and the wave is transmitted only along the lower portion of the array structure, as shown in Fig. 5(b). More details regarding the robustness of the topological edge states are discussed in the Supplementary Material. Our results provide a way to design the novel topological photonic devices with excellent performance using the negative-index media.

The experimental sample based on TLs is constructed according to the scheme in Fig. 3. The experimental setup is shown in Fig. 6(a). The signals are generated by a vector network analyzer (Agilent PNA Network Analyzer N5222A) and then input to the sample, which functions as the source for the system. The normalized transmission spectra for the pseudo-spin-up (red line) and pseudospin-down (blue dashed line) cases are shown in Fig. 6(b). The broadband nature of the topological edge states is indicated by the three bands with high transmittance, consistent with the dispersion relation in Fig. 4(e). In our experiments, the samples are placed on an automatic translation device, allowing the field distribution to be accurately probed using a near-field scanning measurement. The signal is generated from input of a vector network analyzer. A monopole antenna connected to output of the analyzer serves as a near-field probe to record the electric field distribution. The antenna has a length of 1 mm and is placed vertically 1 mm above the TLs to measure the signal from the electric fields of the TLs in the two-dimensional (2D) plane. The spatial distribution of the near field is scanned in steps of 1 mm in both the x and y directions. The field amplitudes are normalized according to their respective maximum amplitudes. Two frequencies of edge states 2.56 and 2.92 GHz are chosen, marked by the green dashed lines in Fig. 6(b). The edge state at 2.56 GHz with pseudospin-up propagates along the upper edge while the edge state with pseudospin-down propagates along the lower edge, as shown in Figs. 6(c) and 6(d), respectively. Similar to Figs. 6(c) and 6(d), the measured electric field E_z distributions of two edge states at 2.92 GHz are shown in Figs. 6(e) and 6(f), respectively. The observed decay of the topological edge states mainly arises from the absorption in the CRLH TLs. Our results not only provide a useful understanding for studying topological structures using metamaterials, but also may pave the way toward realizing broadband topological photonic devices with topological protection in the microwave regime. Furthermore, using the mechanisms of multiple scattering in single negative metamaterials[64,65] or the effective negative coupling coefficient,[66–68]

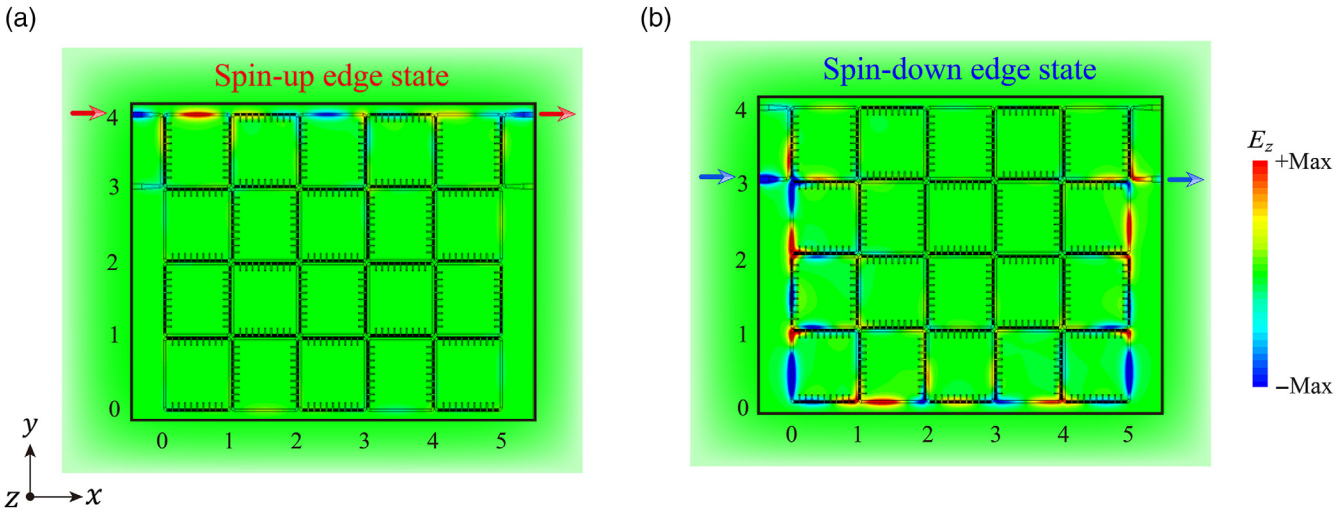

Fig. 5 Simulated electric field E_z distributions of the topological edge states at 2.5 GHz. (a) Simulated E_z distribution when pseudo-spin-up edge state is selectively excited and the electromagnetic wave transports along the upper edge of the structure. (b) Similar to (a), but for the one-way pseudo-spin-down edge state. In this case, the electromagnetic wave is transmitted along the lower edge of the structure.

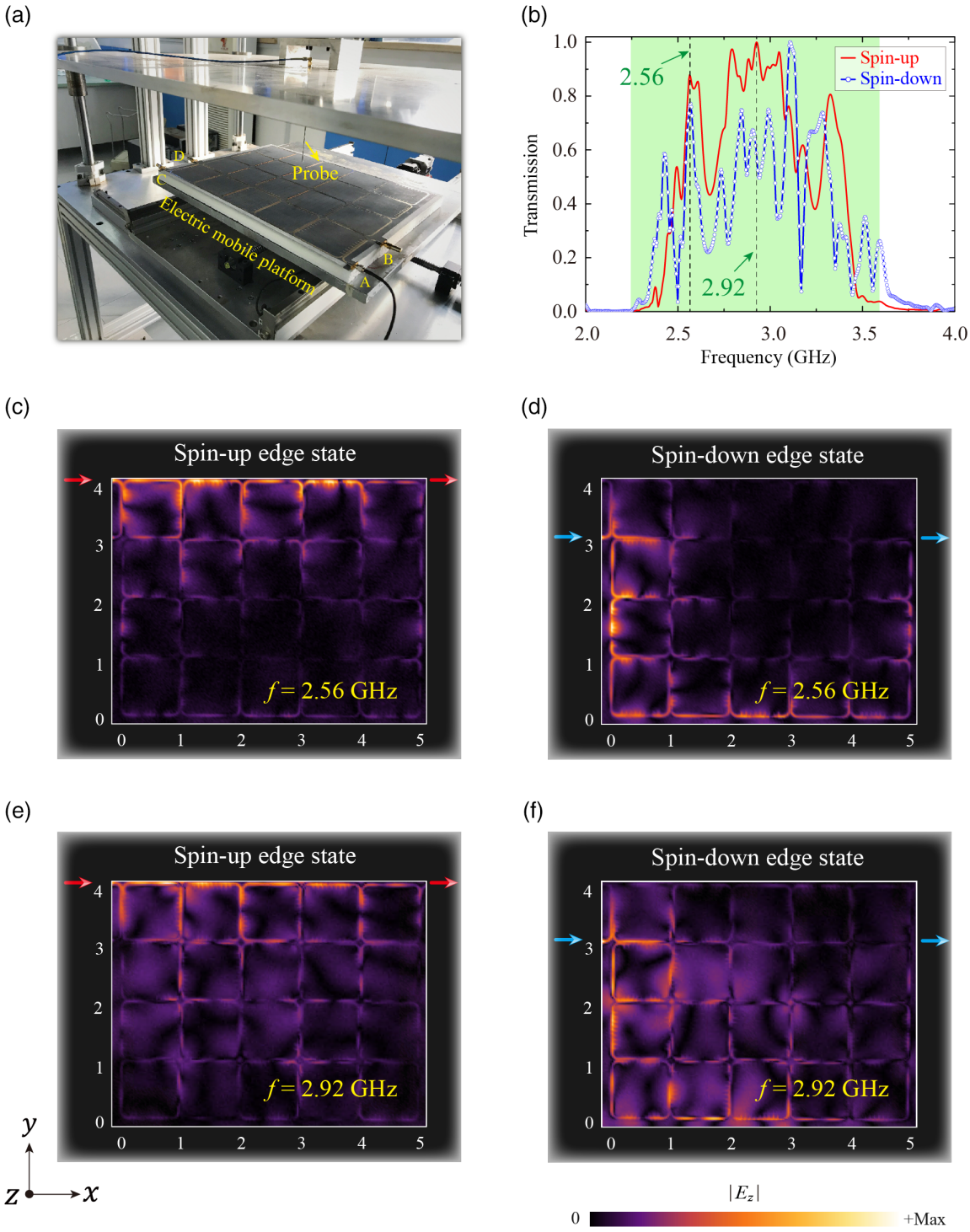

Fig. 6 Experiment setup and observed topological edge states. (a) Photo and diagram of experimental setup for the measurement of the vertical electric field distributions. Our experimental setup is composed of a vector network analyzer, a three-dimensional mobile stage, and the sample to be measured. The sample is put on a 2-cm-thick foam substrate with a permittivity of near 1. The electric probe is a home-made rod antenna, which is connected to the output port of the vector network analyzer. (b) Measured normalized transmission spectra of pseudo-spin-up (red line) and pseudo-spin-down (blue dotted line) cases based on the configuration in panel (a). Measured 2D vertical electric field E_z distributions of the one-way edge states at (c), (d) 2.56 GHz and (e), (f) 2.92 GHz. The exciting position of the pseudo-spin-up (pseudo-spin-down) edge state is marked by the red (blue) arrow.

our design also can be extended to higher frequencies and acoustical systems. In particular, the robustness of topological edge states, such as immunity to structural defects and the ability to pass through sharp corners, is of great interest in the field of microwave engineering. Compared with more traditional microwave devices, whose performance is largely limited by the fabrication difficulty and the tolerance of structural accuracy, photonic devices based on topological edge states have a high tolerance for structural defects and interference. For example, it is well known that sharp bending of coaxial TLs should be strictly avoided in the microwave regime. However, the topological protection mode is not sensitive to the backscattering caused by structural defects. In general, the robustness of the topological edge state makes the photonic topological structure an excellent platform for realizing unique microwave devices, such as isolators, circulators, antennas, delay lines, couplers, and power dividers.[69]

3 Conclusion

In summary, using circuit-based LHM in a TL system, we propose an improved platform to produce an anomalous Floquet topological insulator in a square array of CRLH ring resonators. Additional coupler rings are not necessary, and the resulting topological edge state is broadband in nature. The robustness of topological edge states against a variety of defects has also been verified. Our experimental demonstration of selectively excited one-way edge states will further enrich the design of anomalous Floquet topological insulators and may pave the way toward designing novel photonic topological devices. Moreover, our methods have the potential to explore the topological properties in non-Hermitian systems,[70] which may be useful for some applications, such as beam splitters[71] and funneling of energy.[72]

Acknowledgments

The authors acknowledge the financial support from the National Key R&D Program of China (Grant No. 2021YFA1400602), the National Natural Science Foundation of China (Grant Nos. 12004284, 11974261, 91850206, and 61621001), the Fundamental Research Funds for the Central Universities (Grant No. 22120210579), and the Shanghai Chenguang Plan (Grant No. 21CGA22). The authors declare no conflicts of interest.

References

1. L. Lu, J. D. Joannopoulos, and M. Soljačić, "Topological photonics," *Nat. Photonics* **8**, 821–829 (2014).
2. A. B. Khanikaev and G. Shvets, "Two-dimensional topological photonics," *Nat. Photonics* **11**, 763–773 (2017).
3. T. Ozawa et al., "Topological photonics," *Rev. Mod. Phys.* **91**, 015006 (2019).
4. F. D. M. Haldane and S. Raghu, "Possible realization of directional optical waveguides in photonic crystals with broken time-reversal symmetry," *Phys. Rev. Lett.* **100**, 013904 (2008).
5. Z. Wang et al., "Reflection-free one-way edge modes in a gyromagnetic photonic crystal," *Phys. Rev. Lett.* **100**, 013905 (2008).
6. Z. Wang et al., "Observation of unidirectional backscattering-immune topological electromagnetic states," *Nature* **461**, 772–775 (2009).
7. Y. Poo et al., "Experimental realization of self-guiding unidirectional electromagnetic edge states," *Phys. Rev. Lett.* **106**, 093903 (2011).
8. K. Fang, Z. Yu, and S. Fan, "Realizing effective magnetic field for photons by controlling the phase of dynamic modulation," *Nat. Photonics* **6**, 782–787 (2012).
9. M. C. Rechtsman et al., "Photonic Floquet topological insulators," *Nature* **496**, 196 (2013).
10. A. B. Khanikaev, "Optical physics: on-chip synthetic magnetic field," *Nat. Photonics* **7**, 941–943 (2013).
11. C. L. Kane and E. J. Mele, "Topological order and the quantum spin Hall effect," *Phys. Rev. Lett.* **95**, 146802 (2005).
12. C. L. Kane and E. J. Mele, "Quantum spin Hall effect in graphene," *Phys. Rev. Lett.* **95**, 226801 (2005).
13. A. B. Khanikaev et al., "Photonic topological insulators," *Nat. Mater.* **12**, 233–239 (2013).
14. T. Ma et al., "Guiding electromagnetic waves around sharp corners: topologically protected photonic transport in metawaveguides," *Phys. Rev. Lett.* **114**, 127401 (2015).
15. X. J. Cheng et al., "Robust reconfigurable electromagnetic pathways within a photonic topological insulator," *Nat. Mater.* **15**, 542–548 (2016).
16. C. He et al., "Photonic topological insulator with broken time-reversal symmetry," *Proc. Natl. Acad. Sci.* **113**, 4924–4928 (2016).
17. J. W. Dong et al., "Valley photonic crystals for control of spin and topology," *Nat. Mater.* **16**, 298–302 (2017).
18. L. H. Wu and X. Hu, "Scheme for achieving a topological photonic crystal by using dielectric material," *Phys. Rev. Lett.* **114**, 223901 (2015).
19. Y. Yang et al., "Visualization of a unidirectional electromagnetic waveguide using topological photonic crystals made of dielectric materials," *Phys. Rev. Lett.* **120**, 21740 (2018).
20. X. Zhu et al., "Topological transitions in continuously deformed photonic crystals," *Phys. Rev. B* **97**, 085148 (2018).
21. Y. Li et al., "Topological LC-circuits based on microstrips and observation of electromagnetic modes with orbital angular momentum," *Nat. Commun.* **9**, 4598 (2018).
22. S. Yves et al., "Crystalline metamaterials for topological properties at subwavelength scales," *Nat. Commun.* **8**, 16023 (2017).
23. S. Peng et al., "Probing the band structure of topological silicon photonic lattices in the visible spectrum," *Phys. Rev. Lett.* **122**, 117401 (2019).
24. M. Hafezi et al., "Robust optical delay lines with topological protection," *Nat. Phys.* **7**, 907–912 (2011).
25. M. Hafezi et al., "Imaging topological edge states in silicon photonics," *Nat. Photonics* **7**, 1001–1005 (2013).
26. G. Q. Liang and Y. D. Chong, "Optical resonator analog of a two-dimensional topological insulator," *Phys. Rev. Lett.* **110**, 203904 (2013).
27. M. Pasek and Y. D. Chong, "Network models of photonic Floquet topological insulators," *Phys. Rev. B* **89**, 075113 (2014).
28. X. Zhou et al., "Optical isolation with nonlinear topological photonics," *New J. Phys.* **19**, 095002 (2017).
29. Y. G. Peng et al., "Low-loss and broadband anomalous Floquet topological insulator for airborne sound," *Appl. Phys. Lett.* **110**, 173505 (2017).
30. F. Gao et al., "Probing the limits of topological protection in a designer surface plasmon structure," *Nat. Commun.* **7**, 11619 (2016).
31. G. Harari et al., "Topological insulator laser: theory," *Science* **359**, eaar4003 (2018).
32. M. A. Bandres et al., "Topological insulator laser: experiments," *Science* **359**, eaar4005 (2018).
33. X. Y. Zhu et al., "Z2 topological edge state in honeycomb lattice of coupled resonant optical waveguides with a flat band," *Opt. Express* **26**, 24307 (2018).
34. Y. T. Ao et al., "Topological properties of coupled resonator array based on accurate band structure," *Phys. Rev. Mater.* **2**, 105201 (2018).
35. H. Zhao et al., "Non-Hermitian topological light steering," *Science* **365**, 1163–1166 (2019).

36. S. Mittal et al., "Photonic quadrupole topological phases," *Nat. Photonics* **13**, 692–696 (2019).
37. Q. S. Huang et al., "Observation of the topological edge state in x-ray band," *Laser Photonics Rev.* **13**, 1800339 (2019).
38. Z. K. Shao et al., "A high-performance topological bulk laser based on band-inversion-induced reflection," *Nat. Nanotechnol.* **15**, 67–72 (2019).
39. D. Smirnova et al., "Third-harmonic generation in photonic topological metasurfaces," *Phys. Rev. Lett.* **123**, 103901 (2019).
40. M. A. Gorlach et al., "Far-field probing of leaky topological states in all dielectric metasurfaces," *Nat. Commun.* **9**, 909 (2018).
41. A. Slobozhanyuk et al., "Near-field imaging of spin-locked edge states in all-dielectric topological metasurfaces," *Appl. Phys. Lett.* **114**, 031103 (2019).
42. D. Leykam et al., "Reconfigurable topological phases in next-nearest-neighbor coupled resonator lattices," *Phys. Rev. Lett.* **121**, 023901 (2018).
43. S. Mittal et al., "Photonic anomalous quantum Hall effect," *Phys. Rev. Lett.* **123**, 043201 (2019).
44. M. Li et al., "Higher-order topological states in photonic kagome crystals with long-range interactions," *Nat. Photonics* **14**, 89–94 (2020).
45. Y. H. Yang et al., "Realization of a three-dimensional photonic topological insulator," *Nature* **565**, 622–626 (2019).
46. H. Jia et al., "Observation of chiral zero mode in inhomogeneous three-dimensional Weyl metamaterials," *Science* **363**, 148–151 (2019).
47. B. Yang et al., "Ideal Weyl points and helicoid surface states in artificial photonic crystal structures," *Science* **359**, 1013–1016 (2018).
48. J. Perczel et al., "Topological quantum optics in two-dimensional atomic arrays," *Phys. Rev. Lett.* **119**, 023603 (2017).
49. S. Barik et al., "A topological quantum optics interface," *Science* **359**, 666–668 (2018).
50. S. Mittal, E. A. Goldschmidt, and M. Hafezi, "A topological source of quantum light," *Nature* **561**, 502–506 (2018).
51. C. He et al., "Topological phononic states of underwater sound based on coupled ring resonators," *Appl. Phys. Lett.* **108**, 031904 (2016).
52. Y. G. Peng et al., "Experimental demonstration of anomalous Floquet topological insulator for sound," *Nat. Commun.* **7**, 13368 (2016).
53. S. Afzal and V. Van, "Topological phases and the bulk-edge correspondence in 2D photonic microring resonator lattices," *Opt. Express* **26**, 14567–14577 (2018).
54. S. Afzal et al., "Realization of anomalous Floquet insulators in strongly coupled nanophotonic lattices," *Phys. Rev. Lett.* **124**, 253601 (2020).
55. R. Islam and G. V. Eleftheriades, "A planar metamaterial co-directional coupler that couples power backwards," in IEEE MTT-S Int. Microw. Symp. Dig., Vol. 1, pp. 321–324, IEEE (2003).
56. C. Caloz and T. Itoh, "A novel mixed conventional microstrip and composite right/left-handed backward-wave directional coupler with broadband and tight coupling characteristics," *IEEE Microw. Wirel. Compon. Lett.* **14**, 31–33 (2004).
57. A. Lai, T. Itoh, and C. Caloz, "Composite right/left-handed transmission line metamaterials," *IEEE Microw. Mag.* **5**, 34–50 (2004).
58. Y. Z. Wang et al., "Time-domain study of vortexlike interface mode in metamaterials," *Appl. Phys. Lett.* **91**, 221907 (2007).
59. Z. W. Guo et al., "Focusing and super-resolution with partial cloaking based on linear-crossing metamaterials," *Phys. Rev. Appl.* **10**, 064048 (2018).
60. Z. W. Guo et al., "Anomalous unidirectional excitation of high-k hyperbolic modes using all-electric metasources," *Adv. Photonics* **3**, 036001 (2021).
61. Z. W. Guo, H. T. Jiang, and H. Chen, "Zero-index and hyperbolic metacavities: fundamentals and applications," *J. Phys. D: Appl. Phys.* **55**, 083001 (2022).
62. Y. Sun et al., "Experimental demonstration of a coherent perfect absorber with PT phase transition," *Phys. Rev. Lett.* **112**, 143903 (2014).
63. Z. W. Guo et al., "Enhancement of electromagnetically induced transparency in metamaterials using long range coupling mediated by a hyperbolic material," *Opt. Express* **26**, 627–641 (2018).
64. N. Kaina et al., "Negative refractive index and acoustic superlens from multiple scattering in single negative metamaterials," *Nature* **525**, 77–81 (2015).
65. Z. W. Guo et al., "Photonic spin Hall effect in waveguides composed of two types of single-negative metamaterials," *Sci. Rep.* **7**, 7742 (2017).
66. Y. K. Zhou et al., "Acoustic multiband double negativity from coupled single-negative resonators," *Phys. Rev. Appl.* **10**, 044006 (2018).
67. R. Keil et al., "Universal sign control of coupling in tight-binding lattices," *Phys. Rev. Lett.* **116**, 213901 (2016).
68. Z. Liao et al., "Localized surface magnetic modes propagating along a chain of connected subwavelength metamaterial resonators," *Phys. Rev. Appl.* **10**, 034054 (2018).
69. S. Ma and S. M. Anlage, "Microwave applications of photonic topological insulators," *Appl. Phys. Lett.* **116**, 250502 (2020).
70. S. Y. Yao and Z. Wang, "Edge states and topological invariants of non-Hermitian systems," *Phys. Rev. Lett.* **121**, 086803 (2018).
71. X. Y. Zhu et al., "Photonic non-Hermitian skin effect and non-Bloch bulk-boundary correspondence," *Phys. Rev. Res.* **2**, 013280 (2020).
72. S. Weidemann et al., "Topological funneling of light," *Science* **368**, 311–314 (2020).

Zhiwei Guo received his PhD in physics from Tongji University in 2019. Currently, he is a assistant professor in the School of Physics Science and Engineering at Tongji University. His current research interests include non-Hermitian photonics, topological photonics, circuit-based metamaterials, photonic crystals with metamaterials, metasources for near-field routing, and wireless power transfer.

Biographies of the other authors are not available.